Supplementary materials and methods

Plasmid Constructs. GFP-γ-actin (rat) was provided by Andrew Matus (Friedrich Miescher Institute, Basel, Switzerland). GFP-β-actin (human) and PA-GFP-γ-actin constructs were provided by James Zheng (Emory University, Atlanta, GA). GFP-Utrophin-CH (F-actin probe) and GFP-cortactin (*Xenopus*) were provided by William Bement (University of Wisconsin, Madison). mCherry-Rab5A and DsRed-Clathrin light chain were provided by Jon Audhya (University of Wisconsin, Madison). Paxillin–GFP (chicken) was provided by A. F. Horwitz (University of Virginia, Charlottesville, VA). GFP-α-actinin-1 (human) was provided by Carol Otey (University of North Carolina, Chapel Hill, NC). Human wild-type Tks5 and dominant negative ΔPX-Tks5 tagged with GFP were provided by Sara Courtneidge (Sanford-Burnham Medical Research Institute, La Jolla, CA).

Reagents. SU6656, PP2 and GM6001 were obtained from Calbiochem (La Jolla, CA). MβCD was purchased from Sigma. To visualize F-actin retrograde flow, cultures were loaded with 3 nM kabiramide C conjugated to TMR (TMR-KabC; provided by Gerard Marriott, University of California, Berkeley). Antibodies were used as follows: β1-integrin (8C8), SV2, Znp-1 (Synaptotagmin-2) (Developmental Studies Hybridoma Bank (DSHB)); pY118-Paxillin (44660G), pY397-FAK (44624G), pY418-Src (44660G) (Invitrogen); Cortactin (4F11), MMP14 (AB6005, Millipore); Tks5 (M-300; Santa Cruz Biotechnology), βI,II-Tubulin (T8535) and acetylated-Tubulin (T6793), HNK-1 (C0678, NCAM, Sigma); GFP (Ab6556, AbCAM). Arp3, N-

WASP and Mena were provided by Erik Dent (University of Wisconsin, Madison). Alexa Fluor 488 deoxyribonuclease I (DNase I; Invitrogen) was used to label monomeric G-actin.

Immunocytochemistry. Primary antibodies were diluted in block as follows: 1:250 β-Integrin (8C8), 1:500 pY118-Paxillin, 1:500 pY397-FAK, 1:100 SV2, 1:500 Cortactin, 1:250 Arp3, 1:250 N-WASP, 1:500 Mena, 1:500 pY418-Src, 1:250 Tks5, 1:500 βI,II-Tubulin, 1:1000 acetylated-Tubulin, 1:500 HNK-1 and 1:500 MMP14. Alexa-Fluor-conjugated secondary antibodies (Invitrogen) were used at 1:250 in blocking solution. Alexa-546 phalloidin and Alexa-647 carboxylic acid, succinimidyl ester were used at 1:100 and 1:1000 respectively.

Confocal and TIRF image acquisition and analysis. For both live and fixed fluorescence microscopy *in vitro*, images were acquired using either 60x/1.45NA objective on an Olympus Fluoview 500 laser-scanning confocal system or a 100x/1.49NA objective lens on a Nikon total internal reflection fluorescence (TIRF) microscope. FRAP and FDAP experiments were performed on a Nikon A1 confocal using a 100x/1.45NA objective. On the Olympus confocal, samples were imaged at 2.5x zoom (pixel size = 165 nm). Live explant cultures were sealed within perfusion chambers as described (Gomez et al., 2003) to allow rapid exchange of solutions. Whole mount Z stacks (1-2 um step size) were captured using a 60x/1.1 NA water objective. Images were analyzed using ImageJ software (W. Rasband, National

Institutes of Health, Bethesda, MD) and volumes were rendered using Volocity software.

Structured illumination microscopy image acquisition. High-resolution structured illumination (SIM) Z-stacks were captured using a DeltaVision OMX microscope (Applied Precision), an ELYRA PS.1 microscope (Carl Zeiss Microscopy) or a N-SIM microscope (Nikon). The DeltaVision OMX V4 3D SIM platform with Blaze technology was used with a 60x/1.42 Plan-Apo N objective (Olympus), excitation wavelengths of 488, 561 and 635 nm and 3 sCMOS cameras. Images were acquired using DeltaVision software and deconvolved using softWoRx image processing software (Applied Precision). The ELYRA was used with either a 63x/1.4 Plan-Apochromat or 100x/1.46 α-Plan-Apochromat objective and excitation wavelengths of 488 and 561 nm. N-SIM images were collected on a Nikon Eclipse Ti using a 100x/1.49 CFI Apo TIRF objective using 488 and 561 nm excitation lines. SIM images were collected at 100-200 nm Z-axis steps, with 5-9 rotations of the structured illumination grid were carried out per channel. An iXon 885 EMCCD camera (Andor) was used for acquisition, bearing 8 x 8 μm pixels and a 1004 x 1002 chip resolution. Resulting stacks were processed using default reconstruction parameters in ZEN 2011 software, followed by channel alignment based on measured affine transformation characteristics of the given objective.

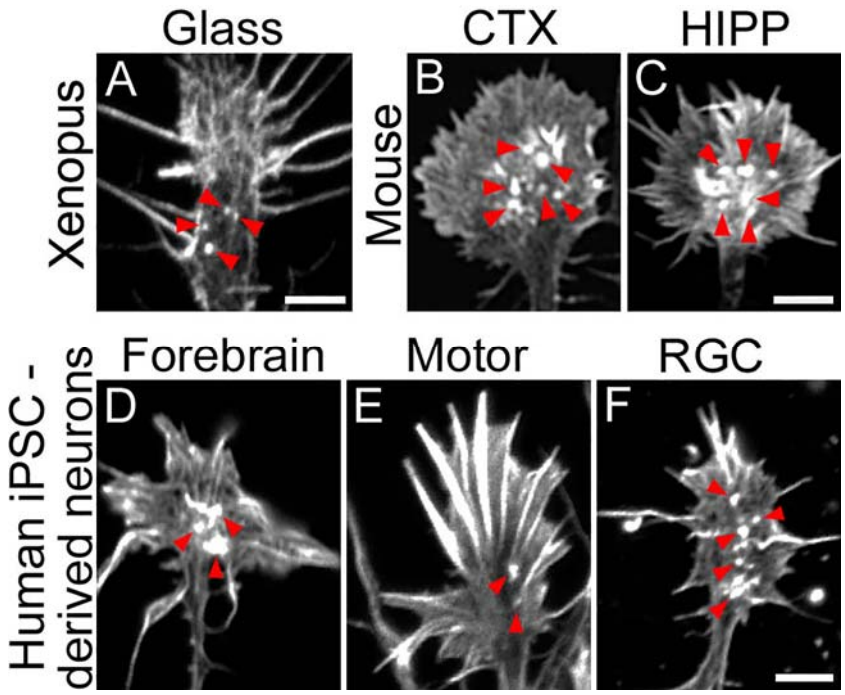

Fig. S1. Mouse and human neuronal growth cones form F-actin rich foci. F-actin in growth cones was labeled with fluorescent phalloidin and imaged by confocal microscopy. **A.** A *Xenopus* spinal neuron growth cone cultured on bare glass. **B-C.** Mouse embryonic cortical (B) and hippocampal (C) growth cones on PDL-L1. **D-F.** Growth cones of human forebrain (D), motor (E) and RGC (F) neurons differentiated from iPSCs and plated on PDL-LN. Note F-actin rich foci located within the C-domain of all growth cones (arrowheads). Scale, 5 μm (A-F).

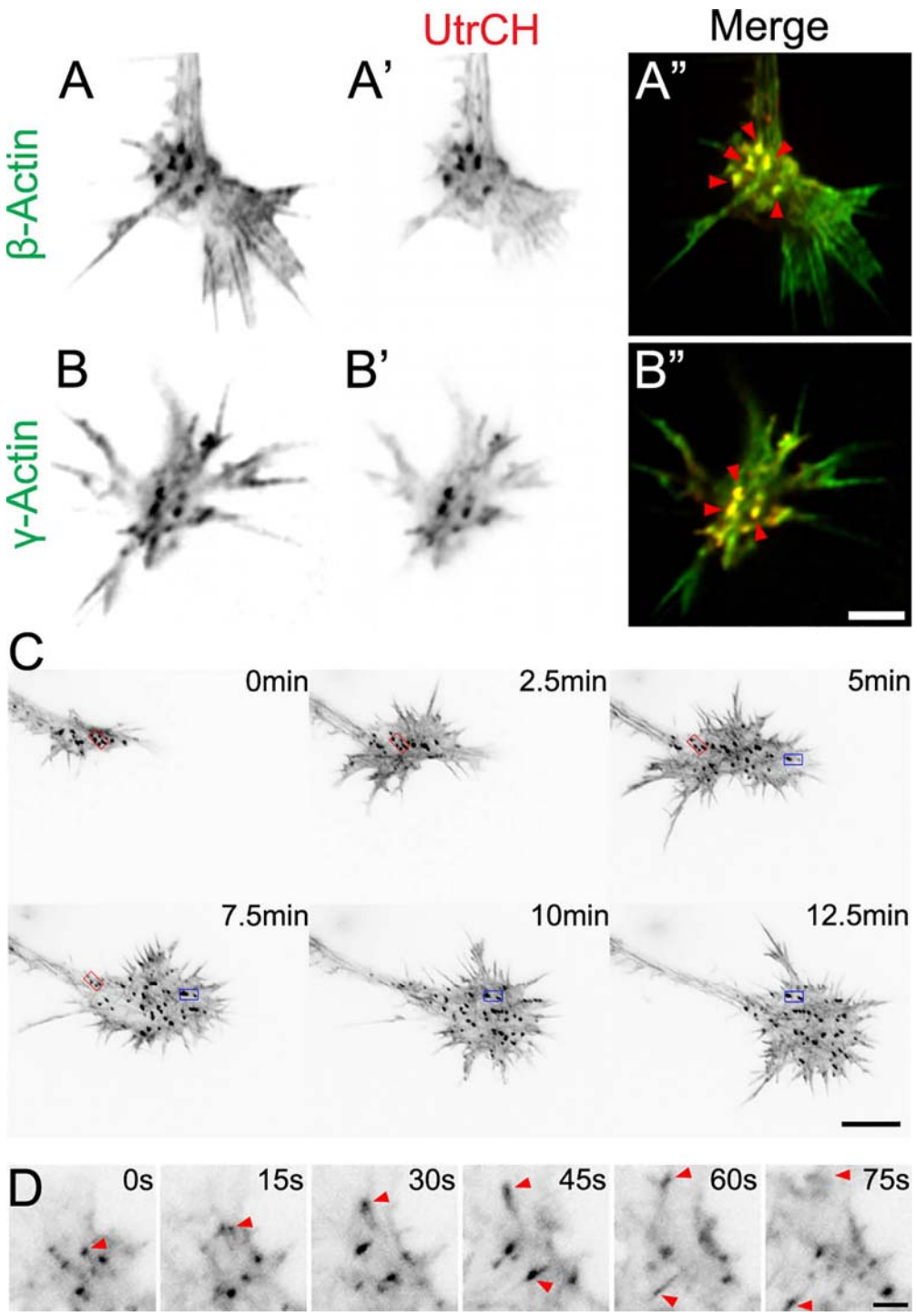

Fig. S2. Both β and γ isoforms of actin target to F-actin rich foci within the C-domain of growth cones. A,B. Live growth cones on LN expressing GFP-β-actin (A) or GFP-γ-actin (B) together with mCh-UtrCH (A', B') imaged by TIRF (inverted contrast). Note in merged images (A", B") that both β-actin

and γ-actin (green) colocalize with mCh-UtrCH (red) labeled F-actin foci (arrowheads). **C.** Time series TIRF images of a live growth cone on LN expressing mCh-UtrCH to label F-actin (inverted contrast). Note that a subset of F-actin foci are highly stable (red and blue boxes). **D**. Time series TIRF images of the leading edge of a growth cone expressing mCh-UtrCH (inverted contrast). Note that some foci appear motile (arrowheads). Scale, 5 μm (A-B), 10 μm (C), 2.5 μm (D).

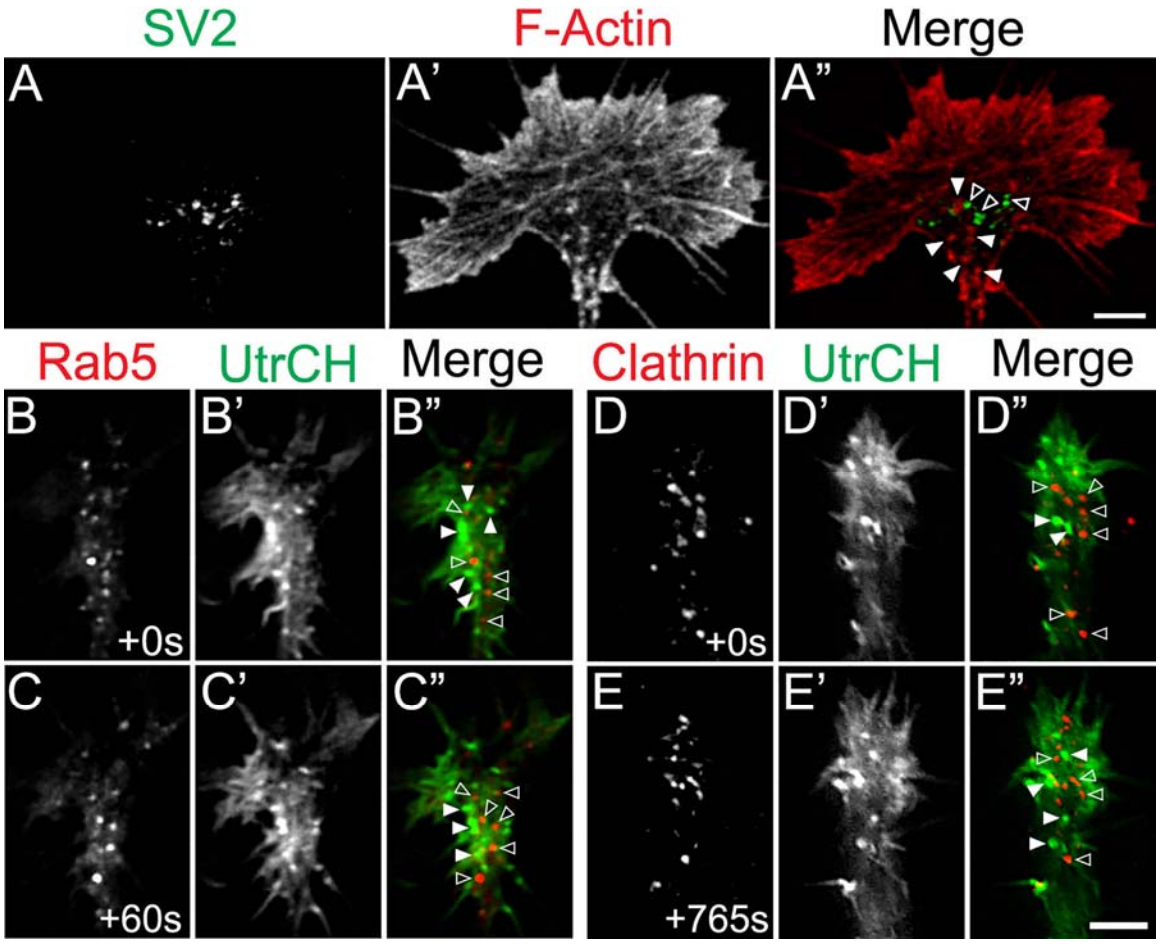

Fig. S3. F-actin foci do not colocalize with exocytotic synaptic vesicles or endocytic vesicles. **A.** Confocal images of a growth cone on LN, immunolabeled for SV2 (A) and F-actin using Alexa-546 phalloidin (A'). **A".** Merged image of SV2 (green) and F-actin (red) shows little colocalization between synaptic vesicles (open arrowheads) and F-actin foci (solid arrowheads). **B-E.** Two time-point TIRF images of live growth cones on LN expressing either mCh-Rab5A (B, C) or DsRed-Clathrin light chain (D, E) and GFP-UtrCH to label F-actin (B'-E'). Note little colocalization between F-actin foci (solid arrowheads, green) and Rab5 or Clathrin (open arrowheads, red). Scale, 5 μm (A-E).

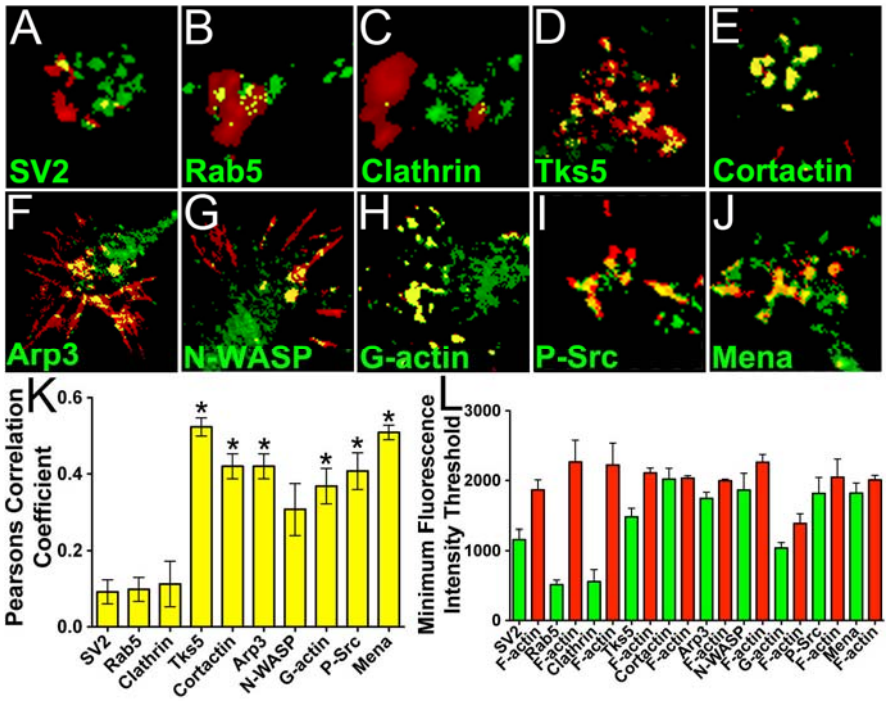

Fig. S4. Quantification of F-actin foci colocalization with various markers by Pearson's correlation coefficient. **A-J.** Specific protein labeling (green) is merged with F-actin labeling with phalloidin (red) for each image. Fluorescent images were thresholded to highlight foci. Little colocalization with F-actin foci (yellow) is observed with SV2 (A), Rab5 (B) or Clathrin (C). However, Tks5 (D), Cortactin (E), Arp3 (F), N-WASP (G), G-actin (H), pY418-Src (I) and Mena (J) all show robust colocalization at F-actin foci. Note that Rab5 and Clathrin were detected as expressed fluorescent fusion protein-conjugates, whereas G-actin was labeled with fluorescent DNase1, and all other proteins were detected by ICC. **K.** The average Pearson's correlation coefficients show significantly greater colocalization of F-actin foci with invadosomal markers compared to each of the vesicle markers. **L.** The average minimum threshold values used to generate Pearson's correlation coefficients for each labeling were not significantly

different. Note that lower minimum intensity thresholds were necessary for mCh-Rab5 and DsRed-Clathrin, as these expressed proteins were dimmer than immunolabelings. *P < 0.05, invadosomal marker compared to vesicle marker, One-way ANOVA, N ≥ 4 growth cones for each marker.

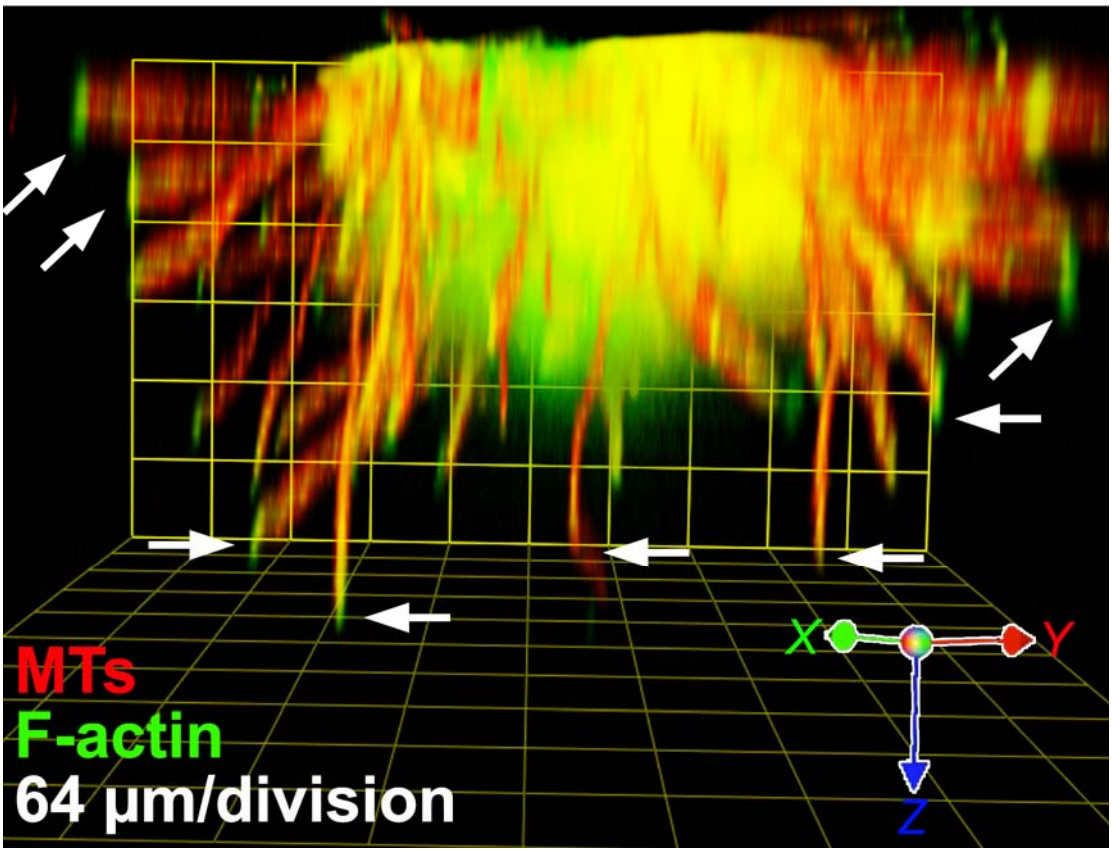

Fig. S5. *Xenopus* spinal axons extend deep into a 3D collagen gel. Confocal Z-series 3D reconstruction of a *Xenopus* spinal explant cultured on top of a collagen-1 gel. The explant was fixed and stained for F-actin with phalloidin (green) and immuolabeled for MTs (red). The deepest axons tipped by growth cones (arrows) extend greater than 300 µm into the gel.

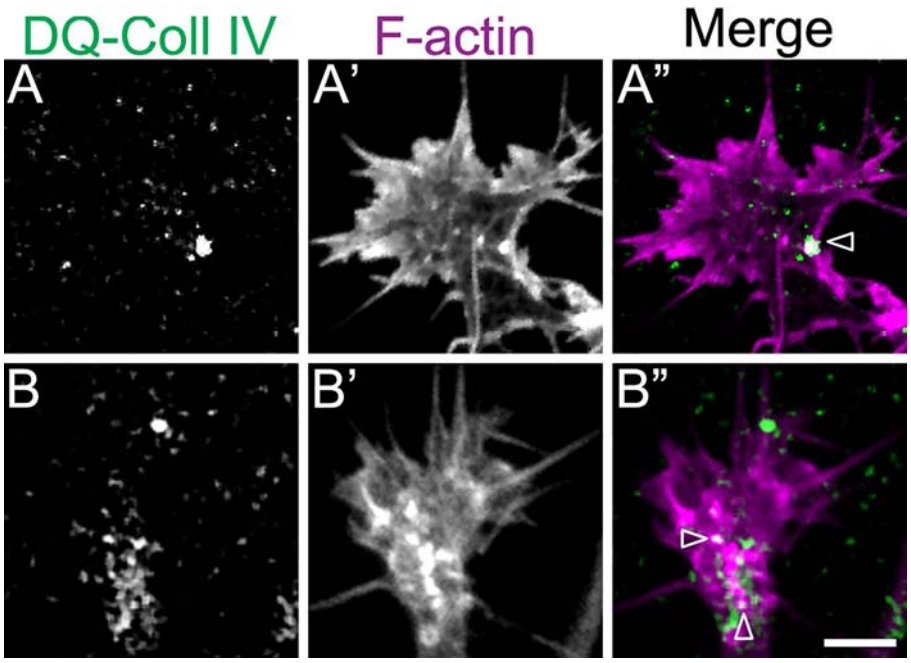

Fig. S6. Growth cone invadosomes are sites of ECM degradation. A, B. Confocal images of spinal growth cones cultured on DQ-collagen IV. **A', B'.** Phalloidin labeling of F-actin. **A", B".** Merged images of the DQ-collagen IV (green) and F-actin label (magenta). Note the colocalization of growth cone invadosomes with areas of collagen degradation visualized as sites of unquenched fluorescence (open arrowheads). Scale, 5 μm (A-B).

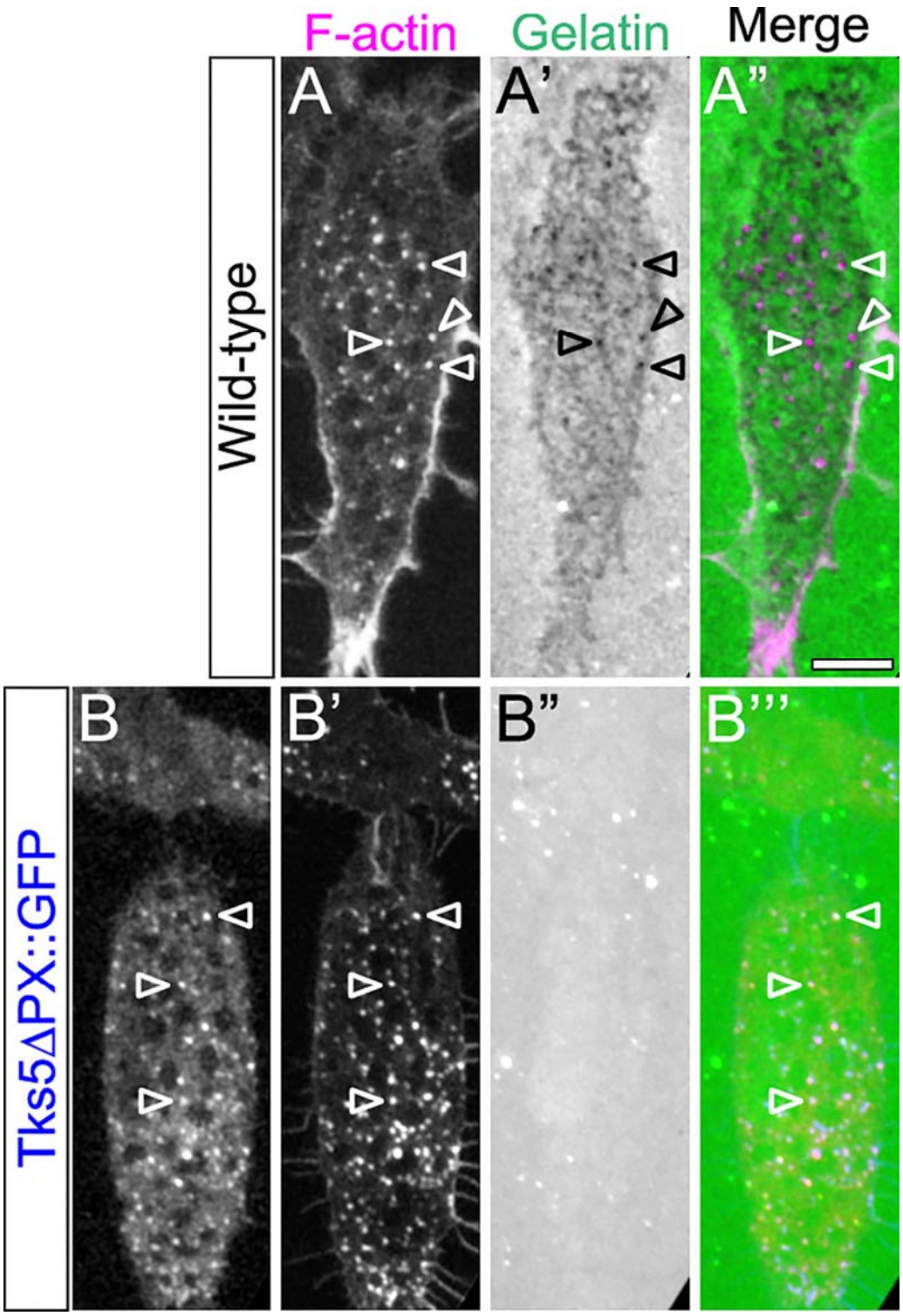

Fig. S7. Dominant negative Tks5, Tks5ΔPX, attenuates gelatin degradation. A-A". Confocal image of a Xenopus neural crest cell on Oregon green 488 gelatin (green in merge), fixed and stained for F-actin (magenta in merge) with Alexa-546 phalloidin. Note the sites of gelatin

degradation under invadosomes in the merge (A"). **B-B"'.** Confocal image of a Xenopus neural crest cell expressing Tks5ΔPX (B, blue in merge) on Cy3-labeled gelatin (B', green in merge), fixed and stained for F-actin (B", red in merge) with Alexa-546 phalloidin. Note the lack of gelatin degradation under invadosomes in the merge (B"'). Scale, 10μm.

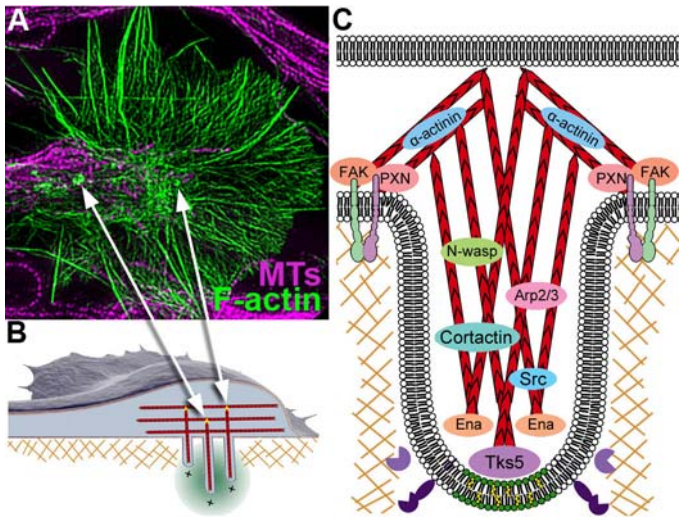

Fig. S8. Model illustrating F-actin rich foci as growth cones invadosomes. **A.** SIM image of a *Xenopus* spinal neuron growth cone on LN, fixed and stained for F-actin (green) with Alexa-568 phalloidin and immunolabeled for βI/II-tubulin (magenta). Note the F-actin rich foci within the growth cone C-domain (arrows). **B.** Illustration of a cross-sectioned growth cone responding to environmental cues by remodeling the ECM with F-actin foci that become protruding invadosomes. Note how invadosomal F-actin orients perpendicular to the planar F-actin network within the growth cone. **C.** Magnified schematic view of a single cross-sectioned growth cone invadosome. Growth cones first establish adhesions with the ECM through the interaction of integrins, Src and adhesion proteins such as paxillin and FAK. Once localized to adhesion sites, Src may phosphorylate Tks5, as well as proteins implicated in lipid raft formation. Phosphorylated Tks5 targets to lipid rafts and initiates actin polymerization through cortactin, N-WASP, the Arp2/3 complex and Ena/Vasp proteins. This network of branched actin assembles F-actin rich columns that span the width of the growth cone and

extend protrusions orthogonal to the plane of outgrowth. Membrane bound and secreted proteases at the tips of invadosomes begin to degrade the ECM, allowing the actin column to transition into a 3-dimensional membrane protrusion. Invadosomal protrusions, formed of both branched and unbranched actin filaments, are stabilized by proteins such as α-actinin. In mature invadosomes, MTs polymerize into the protrusion providing increased stability and the delivery of vesicular cargo, such as proteases and guidance cue receptors. Growth cone invadosomes may represent a novel mechanism for growth cones to respond to environmental cues by remodeling surrounding tissues with 3-dimensional projections during axon guidance.

Movie 1. Growth cones form numerous stable F-actin foci *in vitro* detected by time-lapse GFP-β-actin imaging. Time-lapse TIRF image sequence acquired with a 100X/1.49NA objective of a growth cone on LN expressing GFP-β-actin. This image sequence shows the growth cone from Fig. 1E. Images were captured at 10 sec intervals for 15 min. Playback is 10 frames / sec. Scale bar, 5 µm.

Movie 2. Growth cones form numerous stable F-actin foci *in vitro* detected by time-lapse mCh-UtrCH imaging. Time-lapse TIRF image sequence acquired with a 100X/1.49NA objective of a growth cone on LN expressing mCh-UtrCH, which specifically binds F-actin. This image sequence shows the growth cone from Fig. S2C. Images were captured at 15 sec intervals for 15 min. Playback is 14 frames / sec. Scale bar, 10 µm.

Movie 3. Paxillin targets transiently to F-actin foci. Two channel time-lapse TIRF image sequence acquired with a 100X/1.49NA objective of a growth cone on LN expressing PXN-GFP and mCh-UtrCH. Single channel images are shown as inverse contrast, while merge shows pseudo-colored paxillin (green) and F-actin (red). This image sequence shows the growth cone from Fig. 2E-G. Images were captured at 15 sec intervals for 10 min. Playback is 8 frames / sec. Scale bar, 5 µm.

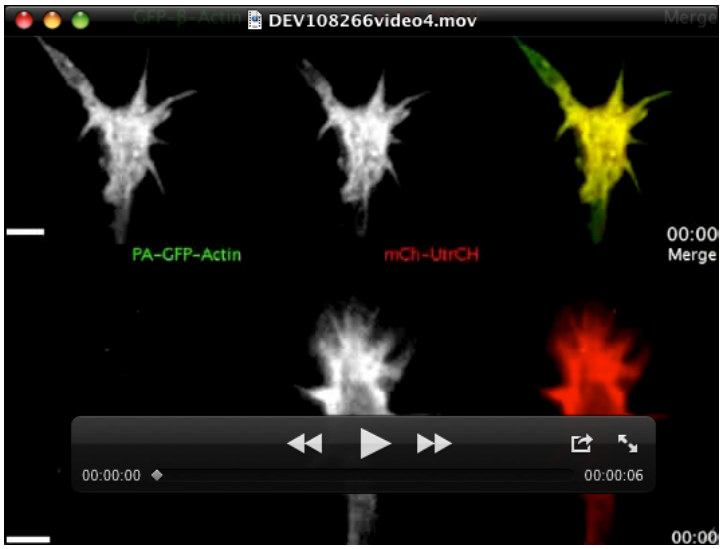

Movie 4. FRAP and FDAP of actin at F-actin foci. Time-lapse confocal image sequence acquired with a 100X/1.45NA objective of growth cones on LN expressing GFP-β-actin and mCh-UtrCH (top) or paGFP-γ-actin and mCh-UtrCH (bottom). This image sequence shows the growth cones from Fig. 3D-F. Images were captured at 1 sec intervals for 64 seconds. Playback is 10 frames/sec. Scale bars, 5 µm.

Movie 5. F-actin foci colocalize with Cortactin. Time-lapse TIRF image sequence acquired with a 100X/1.49NA objective of a growth cone on LN expressing GFP-Cttn and mCh-UtrCH and treated with BDNF. Note Cttn and F-actin colocalize at stable and mobile puncta. Images were captured at 15 sec intervals for 50 min. Playback is 14 frames / sec. Scale bar, 5 µm.

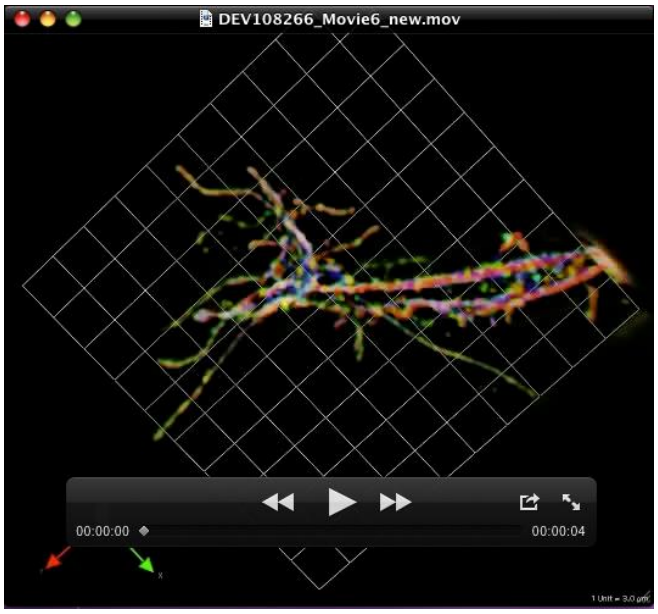

Movie 6. A growth cone in collagen has F-actin foci that are orthogonal protrusions that penetrate into the gel. 3D rotation of a SIM image of a growth cone in a collagen I gel labeled for Cttn (green), MTs (red) and F-actin (blue). Note that Cttn puncta in the central domain of these highly filopodial growth cones are associated with orthogonal protrusions. Image z-series was collected on a Nikon N-SIM microscope. This image sequence shows the growth cone from Fig. 6G.

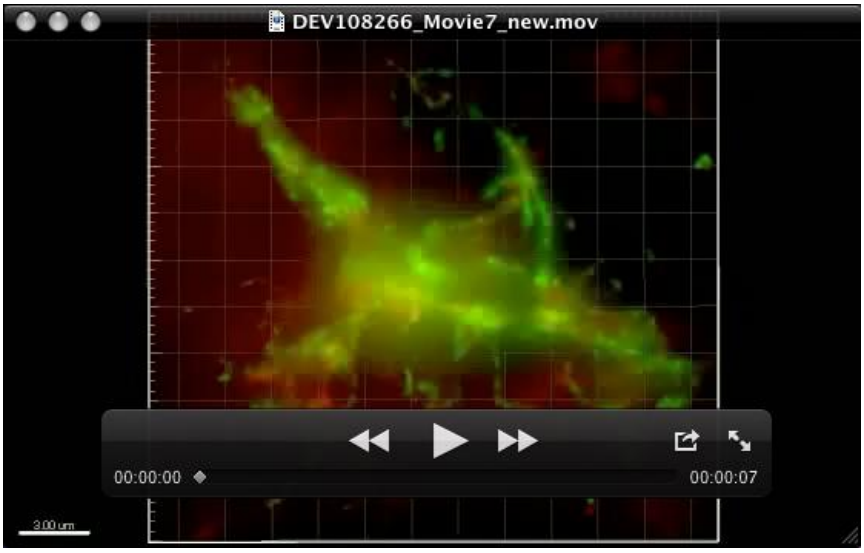

Movie 7. Rohon-Beard growth cones extend invadosome-like protrusions toward the peripheral skin within intact embryos. 3D rotation of a SIM image of a Rohon-Beard growth cone in the peripheral skin of a *Xenopus* embryo labeled for NCAM (Hnk-1, green) and Cttn (red). Note that Cttn puncta near the central domain are associated with orthogonal protrusions that extend toward the skin. Image z-series was collected on a Zeiss ELYRA SIM microscope. This image sequence includes the growth cone depicted in Fig. 7D.

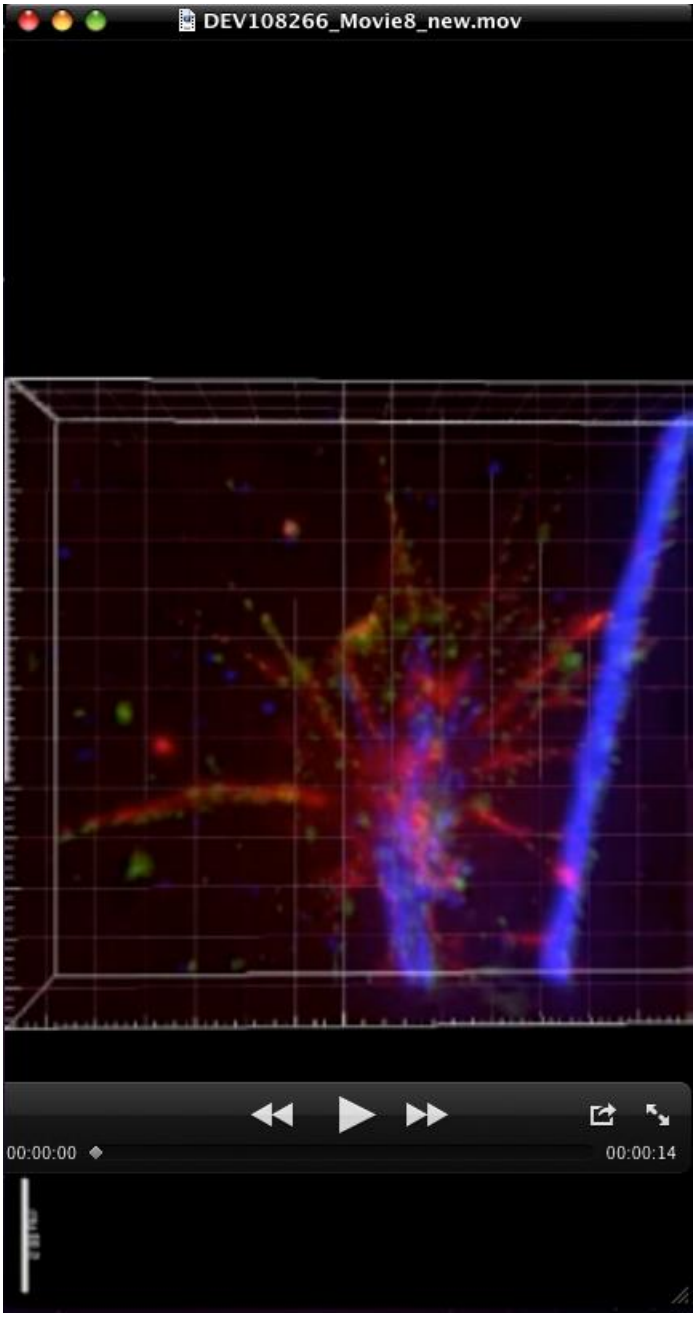

Movie 8. A growth cone with an apical protrusion from the central domain is tipped by ADAM17 MMP. 3D rotation of a super resolution SIM image of a human forebrain neuron growth cone derived from an iPSC on LN immunolabelled for MTs (blue), F-actin (red) and ADAM17 (green). Note that a F-actin foci in the central domain is associated with an apical protrusion that is also ADAM17 positive. Image z-series was collected on a DeltaVision OMX-SIM microscope. This image sequence is the same growth cone shown in Fig. 6E.

Movie 9. GFP-ΔPX-Tks5 clusters into highly mobile puncta within a neural crest cell. Time-lapse TIRF image sequence of a neural crest cell on LN expressing GFP-ΔPX-Tks5. Images were captured at 10 sec intervals for 15 min with a 100x/NA 1.49 objective. Playback is 14 frames / sec. Scale bar, 5 µm.

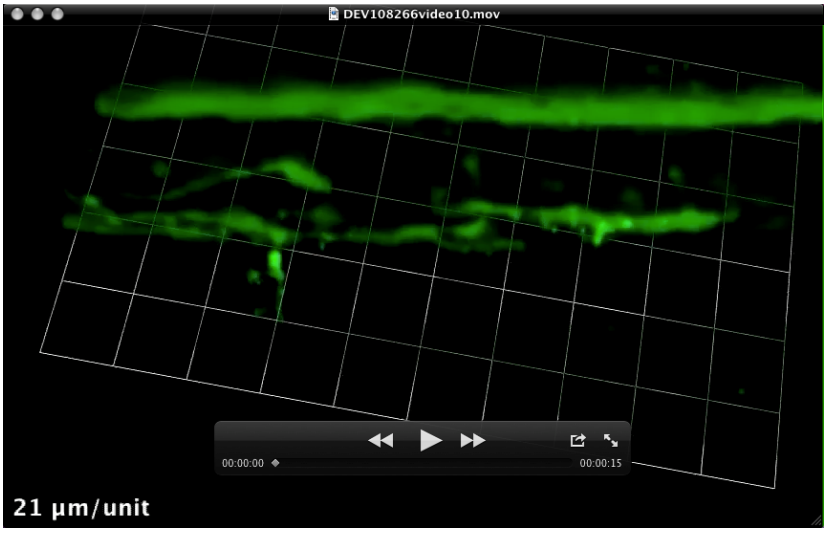

Movie 10. Pioneer MN axons extend invadosome-like protrusions toward the peripheral myotome in vivo. 3D x-axis rotation of a confocal reconstruction of the early spinal cord labeled for synaptotagmin 2 (Znp-1). Note several fine protrusions extend laterally toward the periphery from the terminal of a MN axon on the ventral fascicle.